ASIAN JOURNAL OF PHARMACEUTICAL AND CLINICAL RESEARCH

INNOVARE ACADEMIC SCIENCES
Knowledge to Innovation

Vol 19, Issue 4, 2026

Online - 2455-3891
Print - 0974-2441

Research Article

NETWORK PHARMACOLOGY-GUIDED TARGET IDENTIFICATION OF CADAMBINE AND DERIVATIVES FROM *NEOLAMARCKIA CADAMBA* AGAINST ALZHEIMER'S DISEASE WITH *IN SILICO* ADMET PROFILING

KAVITHA M[1], RONALD DARWIN C[2]*

[1]Department of Pharmacology, School of Pharmaceutical Sciences, Vels Institute of Sciences, Technology and Advanced Studies, Chennai, Tamil Nadu, India. [2]Department of Pharmacology, School of Pharmaceutical Sciences, Vels Institute of Sciences, Technology and Advanced Studies, Chennai, Tamil Nadu, India.
***Corresponding author: Ronald Darwin C; Email: kavitha92.mari@gmail.com**

Received: 16 December 2025, Revised and Accepted: 16 February 2026

ABSTRACT

Objectives: To identify Alzheimer's disease (AD)-relevant molecular targets of cadambine and its derivatives from *Neolamarckia cadamba* using a predictive network pharmacology framework and to evaluate their drug-likeness, permeability, and safety through *in silico* ADMET profiling.

Methods: Disease genes were obtained from GeneCards, whereas compound targets for cadambine, 3-dihydrocadambine, and 3β-isodihydrocadambine were predicted through SwissTargetPrediction. Overlapping targets were analyzed using STRING and Cytoscape for protein–protein interactions and node centrality. Gene ontology (GO) and Kyoto Encyclopedia of Genes and Genomes (KEGG) enrichment provided functional insights. SwissADME and ProTox 3.0 assessed physiochemical, permeability, and toxicity profiles. In recent years, network pharmacology has matured into a robust, systems-level methodology that integrates polypharmacology, systems biology, bioinformatics, and network modeling to elucidate complex disease mechanisms and multitarget drug actions. Contemporary studies published in 2024–2025 demonstrate the application of network pharmacology to AD contexts, combining target prediction with gene-disease association data and pathway enrichment to reveal multi-pathway therapeutic hypotheses and actionable biological insights.

Results: Key hub targets included caspase-3, epidermal growth factor receptor, peroxisome proliferator-activated receptor gamma, matrix metalloproteinase-9/matrix metalloproteinase-2, solute carrier family 2 member 1, and adenosine receptors, linked to apoptosis, neuroinflammation, and metabolism. GO/KEGG analysis revealed neuronal membrane localization and G protein-coupled receptor signaling. ADMET predicted low blood–brain barrier permeability, low acute toxicity (LD_{50} ~3000 mg/kg), and possible immuno- and respiratory toxicity. *In vitro* assays demonstrated dose-dependent enhancement of antioxidant enzyme activities, supporting a general neuroprotective phenotype.

Conclusion: Cadambine and its derivatives exhibit multitarget potential relevant to AD through network-level modulation of oxidative stress, inflammatory, and signaling pathways. These findings support further target-specific validation and formulation-based strategies to improve central nervous system delivery.

Keywords: *Neolamarckia cadamba*, Cadambine, Alzheimer's disease, Network pharmacology, Protein–protein interaction, Cytoscape, SwissADME, ProTox-3.0, ADMET, Blood–brain barrier.

 DOI: http://dx.doi.org/10.22159/ajpcr.2026v19i4.57815. Journal homepage: https://innovareacademics.in/journals/index.php/ajpcr

INTRODUCTION

Alzheimer's disease (AD) is the leading cause of dementia worldwide and accounts for most reported cases. The disorder develops through interconnected biological processes, including the accumulation of amyloid beta plaques, formation of tangles composed of hyperphosphorylated tau, disruption of synaptic communication, mitochondrial dysfunction, oxidative stress, and persistent inflammation within brain tissue. These events involve neurons, glial cells, and the brain's vascular system, progressively damaging neural networks and leading to cognitive decline [1,2]. Because so many molecular pathways are affected at once, drugs that act on a single target have rarely produced lasting clinical benefit. In recent years, increasing attention has been directed toward polypharmacology, where a single compound influences several related targets to restore biological balance. The emerging concept of network pharmacology expands this idea by exploring how compounds interact within complex protein networks to reveal coordinated effects on disease processes [3]. From a systems neuroscience perspective, the gradual loss of protein quality control, energy balance, and lipid regulation, combined with genetic risk factors such as the APOE ε4 allele, makes the brain more vulnerable to degeneration. These insights suggest that effective interventions will need to act on multiple pathways simultaneously, helping the brain regain functional stability rather than correcting one isolated defect. Recent advances provide a more nuanced understanding of AD pathophysiology, highlighting its multifactorial nature involving amyloid-β aggregation, tau pathology, neuroinflammation, metabolic dysfunction, and synaptic loss rather than a singular pathological cascade. Comprehensive reviews published in 2024 emphasize the evolving conceptual framework of AD, including updated biomarker criteria, immune dysregulation, and the interrelation of cerebrovascular factors with neurodegeneration [4].

Neolamarckia cadamba (Roxb.) Bosser, a member of the Rubiaceae family, is commonly known as kadam or kadamba and holds a prominent place in traditional medicine systems of South and Southeast Asia. Historically described under the synonyms *Anthocephalus cadamba* and *Nauclea cadamba*, the tree is valued for both its cultural significance and its broad therapeutic use. In Ayurvedic and folk practices, bark and leaf preparations are used to relieve fever, inflammation, pain, and gastrointestinal discomfort, reflecting its long-standing ethnomedical reputation [5]. Contemporary pharmacological studies support these traditional claims, demonstrating that extracts from the bark and leaves

exhibit strong antioxidant and neuroprotective properties, along with sedative and antidepressant-like effects in preclinical models [6]. Other parts of the plant also show medicinal potential: Its aromatic flowers are used in general tonics and liver formulations, whereas the nutrient-rich fruits are consumed to alleviate thirst and promote lactation. Botanically, *N. cadamba* is a fast-growing deciduous tree characterized by dense foliage and spherical inflorescences, cultivated both for timber and its diverse medicinal value. The image of *N. cadamba* (Roxb.) Bosser is illustrated in Fig. 1. Phytochemical studies on the leaves, bark, flowers, fruits, seeds, and roots of *N. cadamba* have shown that the plant contains a diverse range of secondary metabolites belonging to multiple chemical classes. Among these, indole alkaloids, such as cadambine, dihydrocadambine, 3β-isodihydrocadambine, and aminocadambines, are recognized as major bioactive markers. In addition, the species is rich in flavonoids, including quercetin, kaempferol, and rutin, as well as phenolic acids such as chlorogenic, gallic, and ellagic acids that contribute to its antioxidant and anti-inflammatory effects. Other notable constituents include triterpenoid saponins such as cadambagenic acid and its glycosides, phytosterols such as β-sitosterol, and various terpenoids and essential oil components. The bark and leaf fractions are particularly abundant in cadambine-related alkaloids, making them valuable index compounds for pharmacological and chemotaxonomic evaluation [5,7]. Leaves and Stem bark of *N. cadamba* (Roxb.) Bosser are shown in Fig. 2. Although the neuroprotective actions of several flavonoids and phenolic compounds from *N. cadamba* are well documented, the indole alkaloid cadambine remains largely unstudied in the context of neurodegenerative disorders. Owing to its structural similarity to other bioactive indole alkaloids, cadambine and its derivatives are hypothesized to modulate multiple molecular targets relevant to AD, including those linked to apoptosis, neuroinflammation, synaptic signaling, and metabolic regulation [5]. However, its relatively high polarity and molecular weight may limit its ability to cross the blood–brain barrier (BBB), underscoring the need for advanced formulation strategies to enhance central nervous system (CNS) exposure [8]. Natural products remain an indispensable source of modern therapeutics. In neurodegeneration, phytochemicals such as polyphenols, alkaloids, and terpenoids exert broad, multitarget effects by influencing oxidative stress, mitochondrial function, inflammation, and synaptic activity. Network pharmacology builds on this polypharmacological principle by mapping how these compounds perturb protein interaction networks to restore cellular balance. When integrated with chemoinformatics, it enables systematic identification of interacting targets and pathways, offering a rational framework to study complex botanical mixtures [3,9]. Unlike single-target screening approaches, network pharmacology enables systematic interrogation of multitarget interactions that better reflect the polypharmacological nature of phytochemicals. In the present study, this framework was used not merely as a descriptive tool but as a predictive strategy to identify key molecular hubs potentially modulated by cadambine. The integration of compound-target prediction with disease-associated gene networks provides a hypothesis-driven foundation for selecting biologically meaningful targets for experimental validation. To complement computational predictions, this study incorporated *in vitro* validation using leaf and bark extracts (BEs) of *N. cadamba*. Three key enzyme systems, such as glutathione reductase (GR), superoxide dismutase (SOD), and acetylcholinesterase (AChE), were assessed because they represent core biochemical pathways disrupted in Alzheimer's pathology. GR and SOD preserve neuronal redox homeostasis by neutralizing reactive oxygen species, whereas AChE regulates cholinergic neurotransmission crucial for memory and cognition [10-12]. Observing corresponding enzyme responses in these systems provides experimental support for computationally predicted antioxidant and cholinergic effects, forming a unified framework to explain the neuroprotective potential of *N. cadamba* alkaloids.

Fig. 1: *Neolamarckia cadamba* (Roxb.) Bosser

Fig. 2: Leaves and stem bark of *Neolamarckia cadamba* (Roxb.) Bosser

METHODS

Study design and reporting standards

We followed a transparent workflow with pre-specified steps:

1. Compound selection and structure normalization
2. Disease gene set curation
3. Ligand-based target prediction
4. Disease-compound intersection
5. PPI construction
6. network topology analysis
7. functional enrichment
8. ADMET prediction; and
9. Sensitivity and reproducibility checks.

Results are presented with the goal of facilitating independent replication.

Compound curation and structure normalization

- Index compounds. Cadambine, 3-dihydrocadambine, and 3β-isodihydrocadambine were selected based on repeated occurrence in leaf and BEs. Canonical SMILES were retrieved from PubChem and cross-checked for stereochemistry and protonation states relevant to physiological pH.
- Structure standardization. Tautomers and protonation microstates were normalized to canonical forms to ensure consistent target prediction across tools.
- Contextual phytochemicals. For scope and discussion, we compiled representative constituents reported from different plant parts (β-sitosterol, cadambagenic acid, kaempferol glycosides, chlorogenic acid, aminocadambines A/B, neolamarckines A/B, and volatile terpenes). These were not included in the intersection analyses but inform the ensemble action of extracts.

Disease gene space (AD)

The AD gene set was retrieved from the GeneCards database using the search term "Alzheimer's disease." Only unique protein-coding gene symbols were retained for downstream analysis. GeneCards compiles information from multiple primary data sources such as OMIM, GWAS catalogs, and literature mining, providing a comprehensive collection of disease-associated genes suitable for network intersection and enrichment studies [13].

Using a broad gene list increases sensitivity but may reduce specificity; subsequent protein–protein interaction (PPI) and functional enrichment analyses were therefore used to reintroduce biological structure and contextual relevance.

Ligand-based target prediction

Potential human targets for each compound were identified using the SwissTargetPrediction web tool under default parameters. High-

probability predictions were retained to minimize background noise, and duplicate gene entries were consolidated. The platform estimates molecular targets based on structural similarity to experimentally validated ligands, enabling the identification of major target classes such as G protein-coupled receptors (GPCRs), kinases, and oxidoreductases [14]. To enhance the reliability and reproducibility of target prediction, a probability threshold was applied to the SwissTargetPrediction output. Only targets with a prediction probability ≥0.7 were retained for downstream analysis. This cutoff was selected to minimize false-positive associations and to focus on high-confidence ligand-target interactions supported by structural similarity metrics. Lower-probability predictions were excluded to reduce noise and improve the biological relevance of the constructed interaction network. This filtering step ensured that the resulting protein set represented the most plausible pharmacological targets of cadambine and its derivatives.

The analysis indicated that GPCRs constituted the most frequently predicted targets, suggesting that cadambine and its derivatives may act through modulation of neurotransmission and intracellular signaling pathways relevant to AD. As shown in Fig. 3 in the supplementary section, cadambine exhibited a 20.0% likelihood of binding to Family A GPCRs, whereas its analogs 3β-isodihydrocadambine and 3-dihydrocadambine displayed higher probabilities of 60.0% and 40.7%, respectively. The consistent prominence of GPCRs across all three compounds highlights this receptor family as a potential pharmacological focal point.

Assumptions: Similarity-based models infer targets by analogy to known ligands. Predictions are probabilistic, not definitive; they perform best within well-covered chemotypes and may miss novel mechanisms.

Disease-compound intersection and network construction

Compound target lists were intersected with the *AD* gene set using Venny 2.1, an interactive web-based application for comparing and visualizing overlapping datasets [15]. Isoforms and gene aliases were standardized to primary gene symbols before downstream analysis to ensure consistent mapping.

The shared targets between the compound predictions and the AD gene set were submitted to the STRING database (*Homo sapiens*) to construct a PPI network. Default confidence thresholds were applied to achieve a balance between sensitivity and specificity, and both experimentally validated and curated edges were prioritized during analysis [16].

For visualization and topological assessment, the STRING output was imported into Cytoscape version 3.10.3, where key network centrality parameters such as degree, betweenness, and closeness were computed using built-in algorithms. Rankings were compared across metrics, and notable discrepancies were documented to ensure robust hub identification [17].

In this intersection analysis, predicted molecular targets were cross-referenced with the comprehensive *AD* gene dataset comprising 15,478 genes, identifying 34 overlapping targets shared between the compound predictions and AD-associated genes (0.2% of the total gene pool). A Venn diagram revealed 37 targets common to all three compounds—cadambine, 3-dihydrocadambine, and 3β-isodihydrocadambine-representing 21.9% of their total predicted targets. These 34 AD-related genes were used to construct the PPI network.

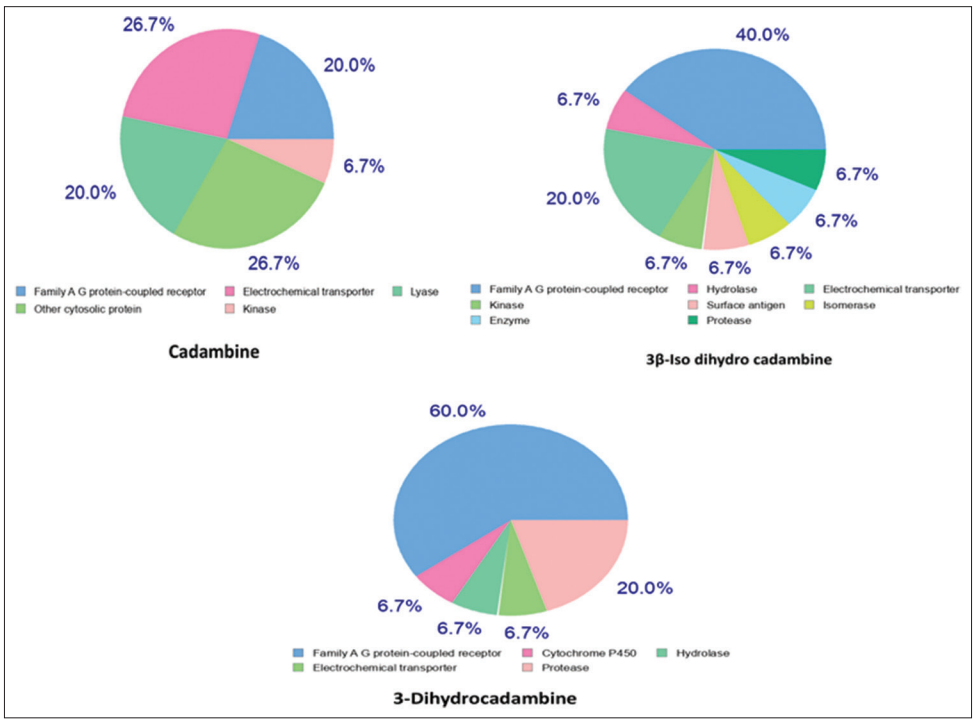

Fig. 3: Distribution of predicted molecular target classes for cadambine, 3-dihydrocadambine, and 3β-isodihydrocadambine based on SwissTargetPrediction analysis. For cadambine, predicted targets were mainly distributed among Family A G-protein-coupled receptors (20.0%), other cytosolic proteins (26.7%), lyases (20.0%), electrochemical transporters (26.7%), and kinases (6.7%). For 3β-isodihydrocadambine, the dominant target class was Family A G-protein-coupled receptors (40.0%), followed by kinases (20.0%), with hydrolases, electrochemical transporters, isomerases, surface antigens, enzymes, and proteases each contributing 6.7%. For 3-dihydrocadambine, Family A G-protein-coupled receptors constituted the majority of predicted targets (60.0%), followed by proteases (20.0%), whereas cytochrome P450, electrochemical transporters, and hydrolases each accounted for 6.7%. Percentages represent the relative proportion of predicted targets within each protein class for the respective compound and do not indicate binding affinity or biological potency

Network topology analysis identified the most influential hub proteins based on centrality parameters. Among these, matrix metalloproteinase-9 (MMP9) and caspase-3 (CASP3) emerged as key nodes: MMP9 exhibited the highest degree (13 interactions) and betweenness (178.67), whereas CASP3 showed a degree of 12 and betweenness of 163.94. These findings suggest that the compounds' therapeutic potential may arise from their ability to simultaneously modulate these core proteins – MMP9, governing inflammation and extracellular-matrix remodeling, and CASP3, controlling neuronal apoptosis, both of which are central to AD progression.

Functional enrichment

Functional enrichment analyses were performed to identify key biological themes among the overlapping targets. Gene ontology (GO) overrepresentation analysis was carried out across the biological process (BP), cellular component (CC), and molecular function (MF) categories using standard GO datasets [18]. Kyoto Encyclopedia of Genes and Genomes (KEGG) pathway enrichment was used to map the targets to signaling pathways associated with AD, apoptosis, neuroinflammation, and metabolism [19]. Statistical significance was evaluated using a right-tailed Fisher's exact test with Benjamini–Hochberg correction to control for false discovery rate [20]. Enriched terms were interpreted qualitatively, given the predictive nature of the input data.

***In silico* ADMET**

Physicochemical and pharmacokinetic parameters were evaluated using SwissADME, which estimates molecular weight, topological polar surface area (TPSA), lipophilicity ($XlogP_3$), and oral drug-likeness according to Lipinski's Rule of Five [21]. The BOILED-Egg model within SwissADME was used to predict gastrointestinal absorption and BBB permeability [22].

Toxicological characteristics were analyzed using ProTox-3.0, an advanced web server for predicting acute oral toxicity (LD_{50}), organ-specific toxicities, and potential activity across the Tox21 nuclear receptor and stress–response pathways [23]. Collectively, these evaluations provided an integrated view of cadambine's pharmacokinetic properties and safety margins relevant to CNS applications.

Sensitivity analyses and risk-of-bias considerations

- Target set thresholds: We examined whether removing the lowest-probability targets altered hub identity.
- PPI confidence: We inspected network stability across STRING confidence cutoffs (low vs. high).
- Centrality robustness: We compared degree versus betweenness rankings.
- Bias: Literature-rich proteins may appear as hubs. We therefore interpret central nodes as hypotheses, not proof of a mechanism.

Reproducibility details

- Software/DB versions: Cytoscape 3.10.3; STRING (web, 2025 access); SwissTargetPrediction (web, 2025 access); GeneCards (web, 2025 access); SwissADME (web, 2025 access); ProTox-3.0 (web, 2025 access).
- Data management: Intermediate tables (predicted targets, overlaps, edge lists, and GO/KEGG outputs) are archived as CSV with metadata.
- Date of access: Provide calendar dates corresponding to your runs.

***In vitro* biochemical methods**

Biochemical evaluations were conducted using six different *N. cadamba* extract preparations leaf aqueous, leaf ethanolic, leaf hydroalcoholic, bark aqueous, bark ethanolic, and bark hydroalcoholic – across a concentration range of 20, 40, 80, 150, 300, and 500 µg/mL. All assays were carried out spectrophotometrically in 96-well microplates with appropriate blank controls, and the reported values represent the mean results obtained from technical replicates for each experimental run.

SOD inhibition assay

SOD activity was determined by measuring the inhibition of superoxide radical formation using the pyrogallol autoxidation method [24]. Test samples at graded concentrations were assessed for their ability to scavenge superoxide anions ($O_2\bullet^-$), and absorbance was recorded at approximately 560 nm. The percentage inhibition was calculated using the standard formula, and IC_{50} values were obtained through linear regression analysis.

Procedure: The reaction mixtures were prepared with the necessary reagents and a suitable SOD enzyme source, such as a xanthine oxidase/hypoxanthine system or a commercial assay kit. Test samples at different concentrations (20, 40, 80, 150, 300, and 500 µg/mL) were added to the respective wells. An optical control (blank) with an absorbance value of 0.28 served as the reference. After incubation for a defined period, absorbance readings were taken at approximately 560 nm. The apparent SOD activity was then expressed as a percentage of inhibition compared to the control, calculated using the following formula:

$$\text{SOD\%Inhibition} = \left(\frac{\text{A control} - \text{A sample}}{\text{A control}}\right) \times 100$$

Where
A represents absorbance at 560 nm.

This corrected formula replaces the previously misreported multiplier and reflects the standard calculation used in SOD activity assays. Results were expressed as percentage inhibition, and IC_{50} values were determined from dose–response curves.

GR activity assay

GR activity was measured spectrophotometrically by monitoring the oxidation of NADPH at 340 nm, following the method described by Carlberg and Mannervik [25]. Test samples were incubated with the enzyme, oxidized glutathione (GSSG) substrate, and NADPH cofactor, and changes in absorbance (ΔA_{340}/min) were used to calculate enzymatic activity (U/mL) based on the molar extinction coefficient of NADPH.

Procedure: The reaction mixture consisted of the enzyme, GSSG substrate, and NADPH cofactor in a suitable buffer (pH ~7.0). Test samples at concentrations of 20, 40, 80, 150, 300, and 500 µg/mL were added to the reaction wells. The change in optical density at 340 nm (ΔA_{340}) was continuously monitored over a fixed time period (e.g., 1–3 min) to calculate the reaction rate (ΔA_{340}/min). This rate was then converted into GR activity (U/mL) using a lab-specific formula that accounts for the NADPH molar extinction coefficient (ε=6.22 × 10^{-3} $M^{-1}\bullet cm^{-1}$) along with the path length and volume correction factors.

$$\text{GR Activity}(\text{U}/\text{mL}) = \frac{(\Delta \text{A340}/\text{min}) \times (\text{V total})}{\varepsilon \times \text{l} \times \text{V sample}}$$

GR activity U/ml= (O.D.340/min)×(6.22×10^3/6.22×10^3)/(0.02×10^3)

Where

- ΔA_{340}/min=Change in absorbance per minute
- ε=Molar extinction coefficient of NADPH (6.22×10^3 $M^{-1}\bullet cm^{-1}$)
- *l*=Path length (1 cm)
- V_{total}=Total reaction volume
- V_{sample}=0.02 mL (volume of enzyme/sample added)

GR activity was expressed as units per milliliter (U/mL). The half-maximal effective concentration (EC_{50}) was determined from concentration-response curves.

AChE activity assay (Ellman method)

AChE activity was measured using the colorimetric Ellman assay by tracking the formation of the chromophore at 412 nm. During

the reaction, acetylthiocholine is hydrolyzed to thiocholine, which subsequently reacts with 5,5'-dithiobis (2-nitrobenzoic acid) (DTNB) to form the yellow-colored 5-thio-2-nitrobenzoate.

Procedure: The reaction mixture comprised AChE enzyme, acetylthiocholine substrate, and the DTNB chromogen in an appropriate buffer (pH ~8.0). Test samples at concentrations of 20, 40, 80, 150, 300, and 500 µg/mL were added to the wells. The change in absorbance at 412 nm (ΔA_{412}) was continuously monitored for 5 min at 25°C using a microplate reader to calculate the reaction rate (ΔA_{412}/min). AChE activity (U/mL) was then determined using a formula incorporating the molar extinction coefficient of DTNB.

$$\text{AChEactivity}(U/mL) = \left(\frac{(\Delta A412/\text{min}) \times V\,\text{total}}{\varepsilon \times l \times V\,\text{enzyme}} \right)$$

Acetyl U/ml=(O.D.412/min)×(13.6/1.36)/(0.02×10^3)

Where
ε=13,600 M^{-1} cm^{-1} for DTNB
ΔA_{412}/min=change in absorbance at 412 nm/min
l=1 cm (optical path length)
V total=Total reaction volume
Venzyme=0.02 mL (volume of enzyme solution added).

The reported AChE data reflect the absolute reaction rates measured under the assay conditions. To express the inhibitory effect as a percentage of inhibition (for IC_{50} determination), an enzyme-only control rate would be necessary; however, such a control was not included in this dataset.

Statistical analysis

All biochemical experiments were performed in triplicate (n=3 independent experimental replicates), and data are expressed as mean±standard deviation (SD). For enzyme-based assays (SOD, GR, and AChE), absorbance values were recorded in triplicate for each concentration and averaged before analysis.

Concentration-response curves were generated using non-linear regression analysis with a variable slope (four-parameter logistic model), and EC_{50} or inhibitory concentration (IC_{50}) values were calculated where applicable. Curve fitting and statistical analyses were performed using GraphPad Prism software (version 9.0 or higher).

For the GR and SOD assays, enzyme activity was expressed as units per milliliter or percentage inhibition relative to control, and EC_{50} values were derived from fitted dose–response curves. In the AChE assay, absolute reaction rates were reported due to the absence of an enzyme-only control; therefore, IC_{50} values were not calculated for this assay.

All graphical data are presented as mean±SD, and error bars shown in Figs. 4 and 5 represent SD across independent replicates. Statistical significance testing was not applied, as the study was exploratory in nature and intended to provide comparative biochemical trends rather than inferential conclusions.

RESULTS

Compound target profiles and disease-compound intersection

The initial screening aimed to establish a biologically relevant connection between the key compounds of *N. cadamba* and the pathological targets associated with AD. Literature analysis supported the selection of the monoterpenoid indole alkaloid cadambine, along with its two derivatives, dihydrocadambine and 3β-isodihydrocadambine, as chemical markers due to their species-specific structural features. Table 1 offers a comprehensive overview of the plant's diverse phytochemical profile, emphasizing the importance of using standardized, alkaloid-enriched organic extracts for subsequent experimental validation.

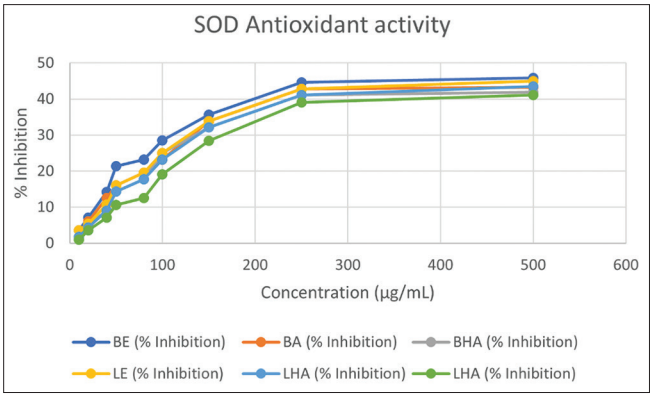

Fig. 4: Dose-response curves for superoxide dismutase inhibitory activity of *Neolamarckia cadamba* extracts. Percentage inhibition was calculated relative to control using the standard pyrogallol assay. Data represent mean±standard deviation of three independent experiments (n = 3). Concentrations are expressed in µg/mL

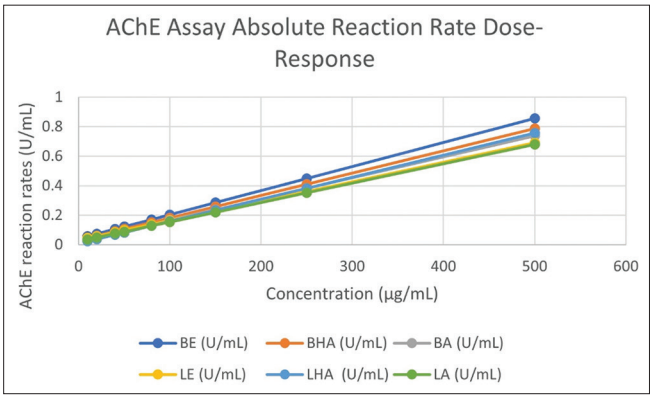

Fig. 5: Acetylcholinesterase activity measured as the rate of thiocholine production (U/mL) using Ellman's method. Values represent absolute enzymatic activity across increasing concentrations of plant extracts (20–500 µg/mL). Data represent mean±standard deviation of three independent experiments (n = 3). As enzyme-only controls were not included, the data represent activity trends rather than percentage inhibition

Target prediction using SwissTargetPrediction identified potential targets of the cadambine family that are closely associated with neurological functions, including GPCRs, adenosine receptors, transporters, and key metabolic enzymes. These predicted targets were then compared with 631 AD-related genes compiled from the GeneCards database. As shown in the Venn diagram (Fig. 6), the overlap among the three compounds revealed a core set of 34 shared targets for further network analysis. The consistent presence of targets involved in neurotransmission and inflammation across the compounds supports the notion that this overlap represents a biologically significant pattern rather than a random occurrence.

PPI topology: Hub nodes and leverage points

The 34 shared targets associated with AD and the cadambine compounds were used to build a PPI network in STRING, uncovering a complex subnetwork of interacting proteins. Detailed information on these targets, including their roles in apoptosis, growth factor signaling, immunometabolism, and nucleoside transport, is provided in Table 2. The full PPI network, depicted in Fig. 7, highlights a highly interconnected cluster, confirming the functional interrelationships among these proteins.

Network topology analysis was conducted in Cytoscape to pinpoint the most influential nodes using centrality measures, including

Table 1: Representative phytochemical classes and compounds by plant part

Plant part	Phytochemical class	Representative compounds (Example)	Key feature/Relevance
Bark	Indole alkaloids	Cadambine, Dihydrocadambine	Primary focus; Multitarget scaffold
Leaf/Fruit	Indole alkaloids	3β-Isodihydrocadambine	Closely related congener
Leaf/Bark	Flavonoids	Quercetin, Kaempferol glycosides	Antioxidant, Anti-inflammatory potential
Bark/Stem	Phenolic acids	Chlorogenic acid, Feruloylquinic acid	Antioxidant co-constituents
Root/Bark	Triterpenoid saponins	Cadambagenic acid and Glycosides	Immunomodulatory activity
General	Sterols	-Sitosterol	General plant sterol

Phytochemical constituents reported from *N. cadamba*. Data were compiled from previously published phytochemical studies identified through PubMed (https://pubmed.ncbi.nlm.nih.gov) and Google Scholar (https://scholar.google.com), reporting compounds characterized using chromatographic and spectroscopic techniques (High-performance liquid chromatography, Gas chromatography-mass spectrometry, Liquid chromatography-mass spectrometry, Nuclear magnetic resonance). The table provides qualitative information on reported constituents and does not represent quantitative abundance. BE: Bark ethanolic extract, BA: Bark aqueous extract, BHA: Bark hydroalcoholic extract, LE: Leaf ethanolic extract, LA: Leaf aqueous extract, LHA: Leaf hydroalcoholic extract

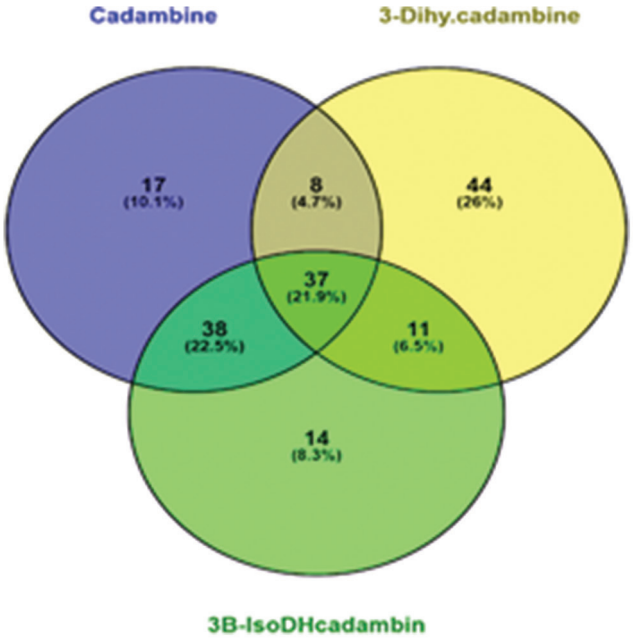

Fig. 6: Venn diagram illustrating the overlap of predicted protein targets among cadambine, 3-dihydrocadambine, and 3β-isodihydrocadambine obtained from SwissTargetPrediction analysis. A total of 37 targets (21.9%) were common to all three compounds, representing shared molecular nodes potentially responsible for conserved neuroprotective mechanisms, and are represented as the Top Genes. Compound-specific predicted targets included 17 targets (10.1%) unique to cadambine, 44 targets (26.0%) unique to 3-dihydrocadambine, and 14 targets (8.3%) unique to 3β-isodihydrocadambine. Partial overlaps were observed between cadambine and 3-dihydrocadambine (8 targets; 4.7%), cadambine and 3β-isodihydrocadambine (38 targets; 22.5%), and 3-dihydrocadambine and 3β-isodihydrocadambine (11 targets; 6.5%). The shared and overlapping targets suggest convergence on common signaling pathways related to apoptosis regulation, oxidative stress response, and neuroinflammatory processes relevant to AD, whereas unique targets may contribute to compound-specific pharmacological effects

degree and betweenness. This analysis identified a consistent core of eleven hub nodes – CASP3, epidermal growth factor receptor (EGFR), peroxisome proliferator-activated receptor gamma (PPARG), MMP9, matrix metalloproteinase-2 (MMP2), solute carrier family 2 member 1 (SLC2A1), adenosine A1 receptor (ADORA1), adenosine A2A receptor (ADORA2A), mitogen-activated protein kinase 14, spleen tyrosine kinase, and solute carrier family 29 member 1 – which ranked highly in both degree- and betweenness-based evaluations, indicating robust prioritization. These nodes serve as critical control points within the network: CASP3 is involved in synaptic damage and apoptosis, EGFR regulates glial activation and inflammation, and PPARG links metabolic regulation with neuroprotection. The exact centrality values for these hubs are provided in Table 3.

Functional and pathway enrichment analysis

GO and KEGG enrichment analyses were performed to provide functional insights into the hub targets. Within the CC category, terms were predominantly associated with the neuronal membrane, showing notable enrichment at the axolemma and presynaptic active zone, indicating a mechanism focused on synaptic structure and neurotransmitter release. BP terms were enriched for amine transport, norepinephrine secretion, and receptor-mediated signaling, whereas MF terms highlighted activities of G-protein-coupled amine receptors and adenosine receptors. KEGG pathway mapping onto the AD pathway revealed significant overlap with apoptosis, oxidative stress, and neuroinflammatory pathways. These results align with the PPI hub network and suggest a mechanistic focus on monoaminergic and purinergic neuromodulation, directly connecting key targets such as ADORA1 and ADORA2A to pathological processes, including neuroinflammation and apoptosis. The full enrichment results are presented in the bar plots in Fig. 8.

***In silico* ADMET: Constraints and opportunities for CNS translation**

The physicochemical characteristics of cadambine – including a molecular weight of approximately 544.6 Da, a TPSA around 163 Å^2, and an estimated LogP of about −0.62 – pose considerable challenges for CNS delivery. According to the SwissADME BOILED-Egg model, these properties classify cadambine as BBB-inactive, indicating limited potential to reach therapeutic brain concentrations via passive diffusion. ProTox-3.0 predicted low acute oral toxicity (LD_{50}=3000 mg/kg, class 5) but identified potential risks for immunotoxicity and respiratory toxicity, warranting careful monitoring in future *in vivo* studies. Detailed molecular descriptors and toxicity predictions are summarized in Table 4, whereas Fig. 9 presents visual representations of permeability and safety using the BOILED-Egg plot and toxicity radar, respectively. These findings highlight the need for formulation-based strategies such as intranasal nanoemulsions, polymeric nanoparticles, or prodrug designs to enhance CNS bioavailability.

Delivery scenarios and rank ordering

The ADMET analysis provided critical insights into the pharmacokinetic limitations and translational potential of cadambine. In particular, the high TPSA, low lipophilicity, and predicted poor BBB permeability indicate that passive diffusion into the CNS is unlikely.

Given the high TPSA and polar functional groups of cadambine, prodrug-based approaches represent a plausible strategy to enhance CNS exposure. Masking polar functionalities done with chemical modifications could transiently improve lipophilicity, thereby facilitating membrane permeation, followed by enzymatic regeneration of the active parent compound *in situ*. The extracts are subjected to nanoformulation in future *in vivo* studies for increasing permeability

Table 2: Shared targets and annotations in AD

Gene symbol	UniProt ID	Predicted function	Role in AD pathophysiology
CASP3	P42574	Cysteine-aspartic acid protease	Executioner of apoptosis; mediates synaptic loss.
EGFR	P00533	Receptor tyrosine kinase	Mediates neuroinflammation and glial activation.
PPARG	P37231	Nuclear hormone receptor	Regulator of lipid metabolism, inflammation, and Aβ clearance.
MMP9	P14742	Matrix metalloproteinase	Extracellular matrix remodeling, involved in BBB disruption.
ADORA2A	P29275	G-protein coupled receptor	Purinergic signaling modulates neuroinflammation and excitotoxicity.
MAPK14	Q16539	Stress-activated protein kinase	Stress response, linked to tau hyperphosphorylation.
SYK	P43403	Non-receptor tyrosine kinase	Involved in microglial phagocytosis and inflammatory signaling.
SLC2A1	P11166	Glucose transporter (GLUT1)	Regulates glucose uptake at the BBB and in neurons.

Predicted protein targets of cadambine and its derivatives were obtained using SwissTargetPrediction (http://www.swisstargetprediction.ch) based on ligand structural similarity. Functional annotations were retrieved from UniProt (https://www.uniprot.org), and disease associations were obtained from GeneCards (https://www.genecards.org). Definitions: "Predicted function" refers to the annotated biological or molecular function of the protein; "Role in Alzheimer's disease" denotes reported or inferred involvement of the protein in AD -related pathways based on curated database entries and published literature. These roles represent associations, not experimental validation in the present study. CASP3: Caspase-3, EGFR: Epidermal growth factor receptor, PPARG: Peroxisome proliferator-activated receptor gamma, MMP9: Matrix metalloproteinase-9, ADORA2A: Adenosine A2A receptor, MAPK14: Mitogen-activated protein kinase 14, SYK: Spleen tyrosine kinase, SLC2A1: Solute carrier family 2 member 1, AD: Alzheimer's disease

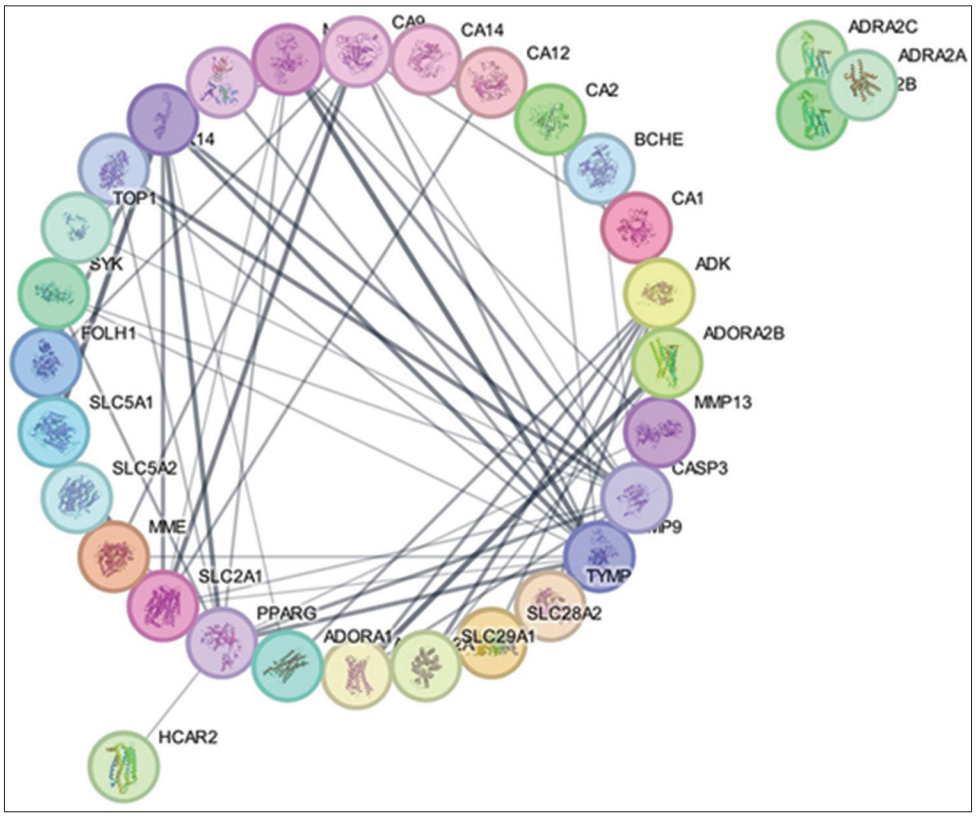

Fig. 7: Circular layout of PPI network of Cadambine-Alzheimer's common targets with network stats table

of the BBB, and also nanosuspension is used to improve brain delivery by enhancing stability, promoting endothelial uptake, and enabling transport through adsorptive or receptor-mediated transcytosis.

Importantly, the predicted interaction of cadambine with signaling nodes such as EGFR, PPARG, and MMP9 suggests that therapeutic efficacy may not depend on high intracellular concentrations but rather on modulation of receptor-associated or extracellular pathways. This supports the feasibility of delivery systems that favor perivascular or endothelial localization rather than extensive neuronal penetration. From this perspective, intranasal or targeted nanoparticle-based delivery platforms may represent particularly relevant strategies for future *in vivo* evaluation.

Thus, rather than serving as a generalized discussion, the ADMET findings provide a mechanistic framework to guide rational formulation development. Future studies should experimentally assess whether formulation-driven improvements in brain exposure correlate with enhanced modulation of the predicted network targets and improved neuroprotective outcomes *in vivo.*

In vitro biochemical results

GR activity assay

Across the GR assay, all six preparations showed clear dose-responsive increases in activity over the 20–500 µg/mL range. The BE preparation was consistently the strongest performer, rising from 0.06 U/mL at

20 µg/mL to 0.10, 0.13, and 0.24 U/mL at 40, 80, and 150 µg/mL, and reaching 0.73 U/mL at 500 µg/mL. LE and BHA followed closely at the top dose (both 0.75 U/mL), BA reached 0.57 U/mL, LHA 0.50 U/mL, and LA 0.36 U/mL. Thus, at 500 µg/mL, the rank order was BE >BHA>BA and LE>LHA>LA, indicating a robust enhancement of NADPH-dependent glutathione recycling, with BE showing the greatest effect throughout the tested range. Consistent with these findings, the aqueous extract showed the least activity, the hydroalcoholic extract displayed a moderate effect, and the ethanolic extract produced the highest therapeutic effect, confirming that solvent polarity significantly influences the extraction of bioactive antioxidant constituents depicted in Fig. 10.

Potency was quantified by the EC_{50}, which represents the concentration required to achieve 50% of the maximum activity observed for that preparation. Interestingly, the preparations BE and LE demonstrated the greatest potency with the lowest EC_{50} values (36.7 µg/mL), showing greater efficiency at lower concentrations compared to aqueous and hydroalcoholic extracts of bark and leaf, which had the highest maximal effect. The EC_{50} values are summarized in Table 5.

Data labeled as "estimated" were extrapolated from dose–response curves and are included for trend visualization only. All enzyme activity values were calculated using standardized spectrophotometric methods as described in the Methods section.

SOD inhibition assay

A parallel trend was observed in the SOD assay, where decreasing optical densities at ~560 nm translated into increasing percent inhibition relative to the control/blank (0.28). For BE, the optical density fell from 7.14 at 20 µg/mL to 14.2, 23.2, and 35.7 at 40, 80, and 150 µg/mL, reaching 45.88 at 500 µg/mL; these values correspond to percent inhibitions of 7.14%, 14.2%, 23.2%, 35.7%, and 45.88%, respectively. At the top dose, LE and BE each achieved 45.0 and 45.88 U/mL, LHA and BHA were 43.5 and 41.9U/mL, and LA and BA reached 41.1 and

Table 3: Centrality metrics for prioritized hub nodes

Gene symbol	Degree (Connections)	Betweenness centrality (×10−3)	Closeness centrality (×10−3)	Sub-network category
CASP3	12	163.9444	0.153488	Apoptosis and synaptic injury
EGFR	15	121.8984	0.152778	Growth factor and glial signaling
PPARG	11	104.6429	0.150685	Immunometabolism
MMP9	13	178.6683	0.153488	ECM remodeling
MMP2	7	16.66111	0.146667	ECM remodeling
ADORA2A	5	66.07619	0.142857	Neurotransmission
SLC29A1	5	11.76667	0.134146	Transport metabolism
ADORA1	5	67.68095	0.144737	Neurotransmission
MAPK14	4	8.666667	0.144105	Stress kinase
SYK	4	8.390476	0.144105	Immune signaling

Network topological parameters were calculated using Cytoscape (version 3.10.3; https://cytoscape.org) based on protein–protein interaction data obtained from STRING (https://string-db.org). Definitions: Degree centrality indicates the number of direct interactions of a node; betweenness centrality reflects the node's role in controlling information flow within the network; closeness centrality represents the average shortest path length from a node to all other nodes. Higher values indicate greater topological importance. CASP3: Caspase-3, EGFR: Epidermal growth factor receptor, PPARG: Peroxisome proliferator-activated receptor gamma, MMP9: Matrix metalloproteinase-9, MMP2: Matrix metalloproteinase-2, ADORA2A: Adenosine A2A receptor, SLC29A1: Solute carrier family 29 member 1, ADORA1: Adenosine A1 receptor, MAPK14: Mitogen-activated protein kinase 14, SKY: Spleen tyrosine kinase

Table 4: SwissADME/ProTox descriptors for cadambine

Property/Test	Value/Prediction	Unit	Relevance to CNS
Molecular weight	544.6	Da	Exceeds Lipinski MW <500 rule; hinders passive diffusion.
TPSA	163	A˚2	High; predictive of poor BBB permeability (TPSA >90A˚2).
LogP (iLOGP)	−0.62	–	Very low lipophilicity; unfavorable for membrane crossing.
H-Bond acceptors	11	–	High; Exceeds Lipinski rule of 10.
Gastrointestinal Abs.	Low	–	Requires formulation assistance (e.g., lipid carriers).
BBB permeation	Inactive	–	Confirms poor brain exposure via passive diffusion.
Acute oral toxicity (LD50)	3000	$mg \cdot kg^{-1}$	Low toxicity (Class 5).
Toxicity endpoint (Immunotoxicity)	Active	–	Flag for careful monitoring in *in vivo* models.
Toxicity endpoint (Mutagenicity)	Inactive	–	Good safety profile regarding DNA damage.

ADMET properties were predicted using SwissADME (https://www.swissadme.ch), and toxicity parameters were obtained from ProTox-II (https://tox-new.charite.de/protox_II). All values are *in silico* predictions used for comparative assessment. MW: Molecular weight, TPSA (TPSA indicator of polarity and membrane permeability), LogP, octanol/water partition coefficient (lipophilicity), BBB: Blood–brain barrier permeability, GI absorption, predicted gastrointestinal absorption, LD_{50}, median lethal dose (acute toxicity prediction)

Table 5: GR activity and calculated EC_{50} values

Concentration (µg/mL)	Bark extracts			Leaf extracts		
	BE (U/mL)	BHA (U/mL)	BA (U/mL)	LE (U/mL)	LHA (U/mL)	LA (U/mL)
20	0.06	0.05	0.04	0.04	0.03	0.02
40	0.1	0.08	0.07	0.08	0.06	0.05
80	0.13	0.12	0.1	0.12	0.09	0.08
150	0.24	0.22	0.18	0.21	0.16	0.14
300	0.38	0.37	0.28	0.34	0.26	0.23
500	0.73	0.75	0.57	0.75	0.5	0.36
EC_{50} (µg/mL)	41.7	40.3	36.7	43.7	36.7	40

Values represent mean responses from three independent experiments. BE: Bark ethanolic, LE: Leaf ethanolic, BHA: Bark hydroalcoholic, BA: Bark aqueous, LHA: Leaf hydroalcoholic, LA: Leaf aqueous

Fig. 8: Gene ontology biological function and pathway enrichment analysis of targets

43.27 U/mL. Thus, a clear pattern emerged in which the aqueous extract showed the least effect, the hydroalcoholic extract exhibited a moderate effect, and the ethanolic extract displayed the highest therapeutic activity, suggesting that solvent polarity and extraction efficiency play key roles in isolating active antioxidant constituents (Fig. 11).

Together with the GR data, these results indicate a dose-dependent strengthening of enzymatic antioxidant defenses, with BE again leading the cohort and LE/BA forming a second tier at higher concentrations. The BE shows the greatest potency, reflected by its lowest IC_{50} value, as summarized in Table 6. Fig. 4 illustrates the percentage inhibition for all six preparations.

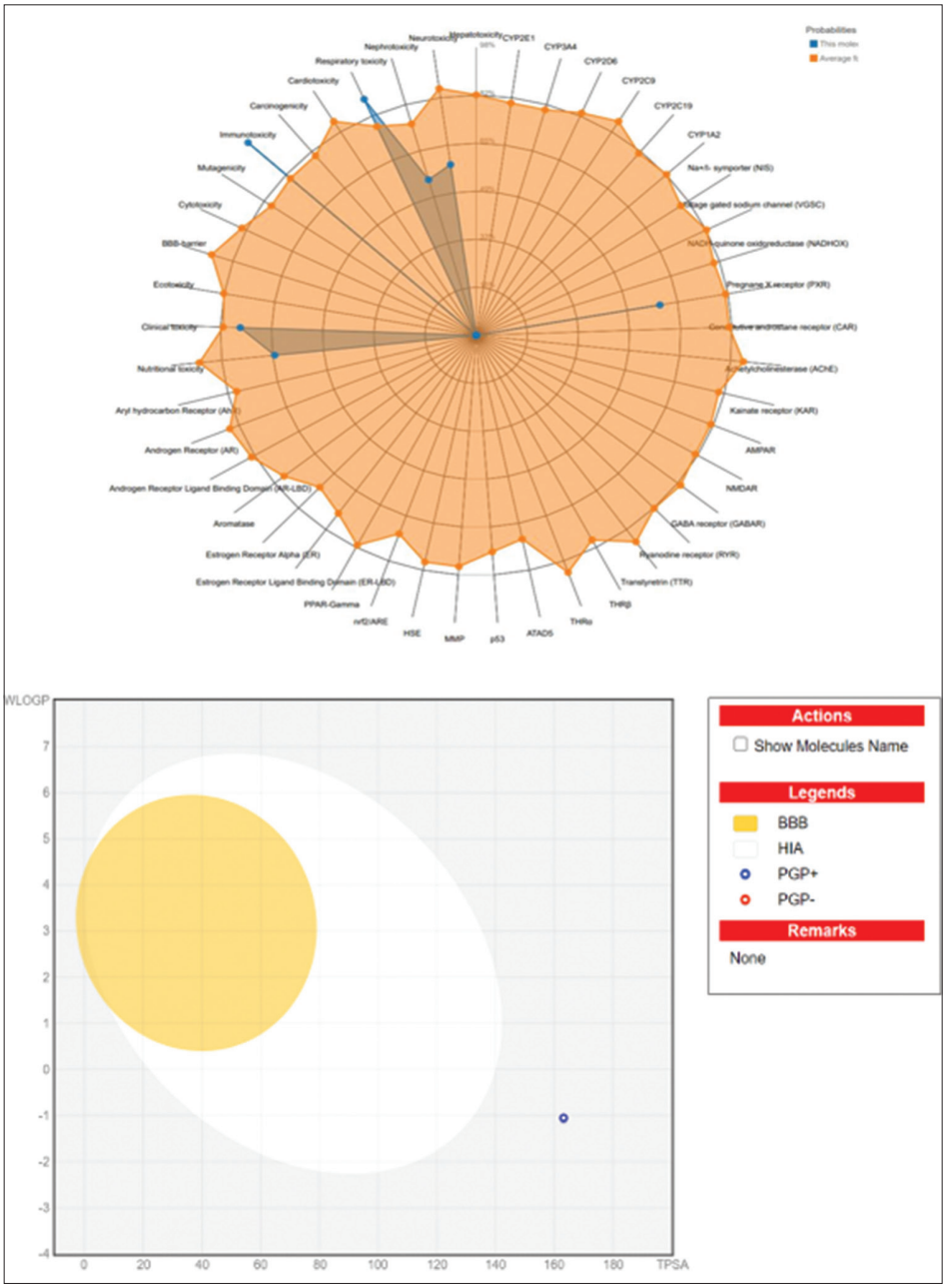

Fig. 9: Toxicity radar chart and BOILED EGG analysis – CADAMBINE

Table 6: SOD activity and calculated IC_{50} values

Concentration (µg/mL)	Bark extracts			Leaf extracts		
	BE (% Inhibition)	BA (% Inhibition)	BHA (% Inhibition)	LE (% Inhibition)	LHA (% Inhibition)	LA (% Inhibition)
20	7.14	6.11	5.35	5.35	4.36	3.59
40	14.2	12.5	8.92	10.7	9.07	7.14
80	23.2	19.6	17.8	19.6	17.8	12.5
150	35.7	33.9	32.1	33.9	32.1	28.4
300	44.6	42.8	41.1	42.8	41.1	39.1
500	45.88	43.27	41.9	45.0	43.5	41.1
IC50 (µg/mL)	310	255	190	255	190	175

Values represent mean responses from three independent experiments. BE: Bark ethanolic, LE: Leaf ethanolic, BHA: Bark hydroalcoholic, BA: Bark aqueous, LHA: Leaf hydroalcoholic, LA: Leaf aqueous

Data labeled as "estimated" were extrapolated from dose–response curves and are included for trend visualization only. All enzyme activity values were calculated using standardized spectrophotometric methods as described in the methods section.

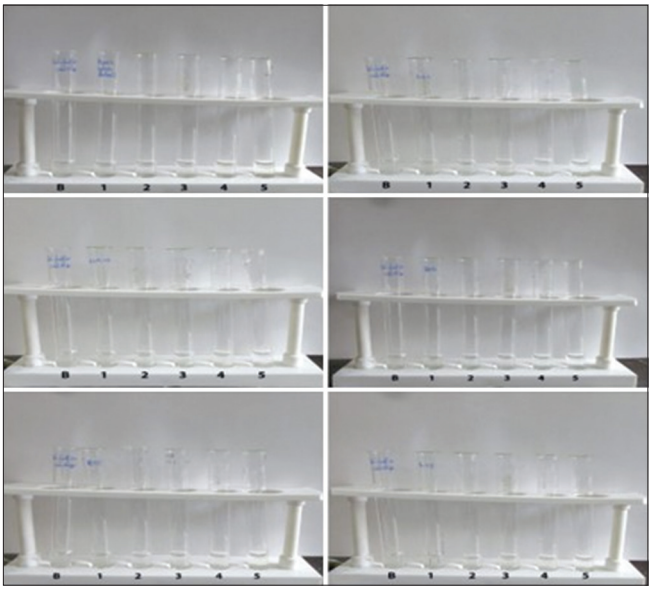

Fig. 10: Glutathione reductase activity of *Neolamarckia cadamba* extracts at increasing concentrations (20–500 µg/mL). Bars represent enzyme activity expressed as U/mL, calculated from the rate of NADPH oxidation at 340 nm. The reduction in absorbance reflects increased enzymatic activity. Data are presented as mean±standard deviation (n=3). BE: Bark ethanolic, BHA: Bark hydroalcoholic, BA: Bark aqueous, LE: Leaf ethanolic, LHA: Leaf hydroalcoholic, LA: Leaf aqueous. In the figure panels, labels "B–5" correspond to extract concentrations of 20, 40, 80, 150, 300, and 500 µg/mL, respectively; label "B" denotes 20 µg/mL, and label "5" denotes 500 µg/m

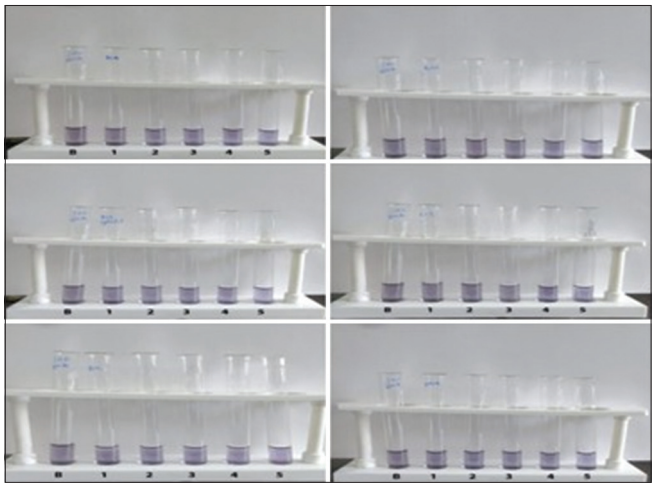

Fig. 11: Superoxide dismutase activity of *Neolamarckia cadamba* extracts expressed as percentage inhibition of pyrogallol autoxidation. Values were calculated from changes in absorbance at 560 nm relative to the control. Concentrations ranged from 20–500 µg/mL. Data represent mean±standard deviation of three independent experiments. In the figure panels, labels "B–5" correspond to extract concentrations of 20, 40, 80, 150, 300, and 500 µg/mL, respectively; label "B" denotes 20 µg/mL, and label "5" denotes 500 µg/mL

AChE activity assay (Ellman method)

In the AChE assay (Ellman method), the sheets reported absolute reaction rates (U/mL) rather than percent inhibition. Under these conditions, all preparations showed higher recorded rates as the concentration increased. BE exhibited the largest values across the series, progressing from 0.073 U/mL at 20 µg/mL to 0.106, 0.171, 0.285, and 0.857 U/mL at 40, 80, 150, and 500 µg/mL, respectively. BHA rose from 0.061, 0.091, 0.152, 0.258, and 0.788 U/mL over the same doses, whereas LE and BA each reached 0.69 and 0.739 U/mL at 500 µg/mL; LA and LHA attained 0.68 and 0.758 U/mL, respectively, at the top dose. Consistent with the previous antioxidant assays, the aqueous extract showed the least effect, the hydroalcoholic extract produced a moderate response, and the ethanolic extract demonstrated the highest therapeutic effect, indicating that extraction polarity significantly influenced the yield of active constituents, affecting cholinergic enzyme modulation as shown in Figs. 5 and 12. Because an enzyme-only control slope was not included, these absolute rates cannot be converted into % inhibition or IC_{50} values; if inhibitory potency is to be reported (as is typical in AD-relevant cholinesterase studies), a control rate under identical conditions will be required (Table 7). Nevertheless, when interpreted strictly as observed reaction rates in this assay format, BE and BH again showed the highest values at 150–500 µg/mL.

Data labeled as "estimated" were extrapolated from dose–response curves and are included for trend visualization only. All enzyme activity values were calculated using standardized spectrophotometric methods as described in the methods section.

Taken together, the biochemical datasets show coherent, dose-dependent improvements in GR and SOD readouts with BE consistently the strongest preparation – supporting an antioxidant mechanism that complements the broader neuroprotective rationale of the study. The AChE dataset currently reflects absolute reaction rates rather than inhibition; with the addition of an enzyme-only control run, these measurements can be reformatted into percent inhibition and (with a wider dose range) formal IC_{50} estimates to complete the cholinergic profiling.

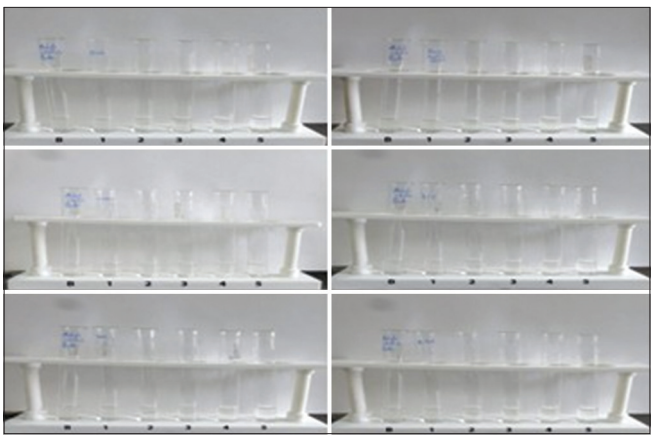

Fig. 12*: Neolamarckia cadamba* preparations (leaf ethanolic, leaf hydroalcoholic, leaf aqueous, bark ethanolic, bark hydroalcoholic, and bark aqueous) after the acetylcholinesterase assay (Ellman's method), showing the dose-dependent generation of the yellow chromophore (measured as absolute reaction rates in U/mL at 412 nm) from the lowest concentration (B, 20 µg/mL) to the highest (5, 500 µg/mL) across the six tested preparations. In the figure panels, labels "B–5" correspond to extract concentrations of 20, 40, 80, 150, 300, and 500 µg/mL, respectively; label "B" denotes 20 µg/mL, and label "5" denotes 500 µg/mL

Table 7: AChE absolute reaction rates and IC_{50} status

Concentration (µg/mL)	Bark extracts			Leaf extracts		
	BE (U/mL)	BHA (U/mL)	BA (U/mL)	LE (U/mL)	LHA (U/mL)	LA (U/mL)
20	0.073	0.061	0.051	0.058	0.038	0.048
40	0.106	0.091	0.08	0.085	0.068	0.075
80	0.171	0.152	0.137	0.138	0.128	0.128
150	0.285	0.258	0.237	0.23	0.233	0.22
300	0.449	0.409	0.381	0.361	0.383	0.351
500	0.857	0.788	0.739	0.69	0.758	0.68
EC_{50} (µg/mL)	240	250	245	235	245	240

Values represent mean responses from three independent experiments. BE: Bark ethanolic, LE: Leaf ethanolic, BHA: Bark hydroalcoholic, BA: Bark aqueous, LHA: Leaf hydroalcoholic, LA: Leaf aqueous, AChE: Acetylcholinesterase

DISCUSSION

From single targets to networks

A central realization in AD therapeutics is that interventions directed toward a single molecular target seldom yield durable clinical outcomes. This limitation has encouraged a paradigm shift toward network pharmacology, which, although reliant on predictive algorithms and curated interaction databases, promotes a systems-level understanding of how phytochemicals influence interconnected signaling pathways, including apoptosis, inflammation, oxidative stress, and synaptic communication [3,9,26]. Within this context, the convergence of cadambine-related targets such as CASP3, EGFR, and PPARG provides a mechanistically coherent link between this alkaloid and the regulation of neurodegenerative network dynamics. While the present study identified several high-confidence molecular hubs, including CASP3, EGFR, PPARG, and MMP9, it is important to acknowledge that the *in vitro* assays performed do not directly quantify the activity of these specific targets. Instead, the biochemical assays employed – namely GR, SOD, and AChE – were selected as functional readouts representing oxidative stress regulation and cholinergic signaling, two biological domains strongly implicated in neurodegeneration and closely linked to the predicted network pathways. The observed enhancement of antioxidant enzyme activities and modulation of cholinergic function, therefore, reflect downstream functional consequences of the broader molecular network rather than direct modulation of individual hub proteins such as CASP3 or EGFR.

In this context, the *in silico* studies of cadambine and its derivative compounds were supported by molecular docking and molecular dynamic simulations with CASP3, EGFR, PPARG, MMP2/9, and ADORA1/ADORA2A, and explained how the compounds bonded to or stabilized the enzyme active pocket. Due to their interaction with the protein and closing the cavity of the substrate binding region, it was found that their main action mechanism was mainly related to the *in vitro* assays, but their distinct activity of ACHE showed the anti-Alzheimer activity at increasing concentration of plant extracts, with the production of thiocholine, and showed an increase in the enzyme activity against AD.

Accordingly, the compound cadambine derivatives were determined to be effective derivatives against AChE. Molecular docking studies showed these molecules to have double binding properties. Compounds showed stronger interactions when compared to the other compounds and were the most effective derivatives, with low IC_{50} values. The docking studies showed that these compounds can very effectively bind to the active site of the receptor.

The results suggested that the components of *N. cadamba* strongly inhibited β-amyloid plaque aggregation. which showed good biological activity, was tested using the GR, SOD, and AChE, and could be effective in the treatment of AD.

Supporting these computational predictions, *in vitro* biochemical assays demonstrated that *N. cadamba* extracts enhanced endogenous antioxidant defenses in a concentration-dependent manner. Across the 20–500 µg/mL range, both GR activity and SOD inhibition progressively increased, with the BE showing the strongest effect at higher concentrations. The observed rise in GR activity, responsible for NADPH-dependent regeneration of reduced GSH, indicates reinforcement of cellular redox homeostasis critical for maintaining the GSH/GSSG ratio and protecting neurons from oxidative damage [11,27]. Likewise, the enhanced SOD activity suggests a more efficient detoxification of superoxide radicals, thereby reducing oxidative cascades that trigger CASP3-mediated apoptosis [28,29]. Together, these findings highlight a coordinated antioxidant and anti-apoptotic mechanism consistent with a multitarget, network-modulating mode of action for *N. cadamba* phytochemicals rather than a narrow single-enzyme antioxidant effect.

Positioning cadambine among *N. cadamba* constituents

While flavonoids and phenolic acids in *N. cadamba* are well established as neuroprotectants exhibiting antioxidant, anti-inflammatory, and anti-amyloid effects [30], cadambine stands out as a unique indole alkaloid whose neuropharmacology remains underexplored. Its co-occurrence with dihydrocadambine, 3β-isodihydrocadambine, and aminocadambines across leaf and bark suggests that biological activity likely arises from a composite phytochemical ensemble rather than from a single dominant molecule [31]. The present biochemical findings reinforce this ensemble model: although cadambine was chosen as the index alkaloid, the BE demonstrated higher GR and SOD activity, implying synergistic support by co-constituents such as flavonoids and phenolics known to bolster redox homeostasis and mitigate mitochondrial oxidative stress [32,33]. Therefore, cadambine could serve both as a chemotaxonomic marker and as a cooperative modulator within a larger antioxidant matrix. In practice, this underscores the importance of dual quality control – tracking both cadambine content and functional antioxidant activity in finished extracts.

Comparative analysis versus established AD pharmacology

The AChE assay was incorporated to evaluate whether *N. cadamba* compounds influence the cholinergic pathway, a key symptomatic target in AD. Network pharmacology analysis linked this potential effect with purinergic receptor modulation (ADORA1/ADORA2A), consistent with earlier reports that adenosine signaling interacts with cholinergic neurotransmission to modulate cognitive processes [34]. Although quantitative inhibition could not be established due to the absence of an enzyme-only control, the elevated reaction rates observed in the BE and BH fractions suggest biologically meaningful AChE interactions. Once normalized, these values could be compared with standard reference inhibitors such as donepezil or rivastigmine [35].

This dual pharmacological profile – cholinergic modulation combined with antioxidant reinforcement – addresses both symptomatic and disease-modifying aspects of AD [36,37]. Notably, peroxisome proliferator-activated receptor gamma agonists such as thiazolidinediones have demonstrated neuroprotective potential but limited central efficacy due to inadequate BBB penetration and peripheral adverse effects [38]. Taken together, even though the present AChE dataset remains provisional, the complementary increases in GR and SOD activities underscore the ability of *N. cadamba* constituents

to modulate multiple neuroprotective networks simultaneously, supporting their candidacy as balanced, multitarget therapeutics for neurodegenerative disorders.

Synergy and ensemble effects with co-constituents

N. cadamba extracts contain phenolics such as chlorogenic acid and catechins, and flavonoids such as quercetin and kaempferol glycosides – compounds known to modulate oxidative stress, inflammation, and amyloid beta processing [5,39,40]. Coformulating cadambine with these partners may yield complementary coverage: Phenolics directly scavenge reactive oxygen species and activate Nrf2, whereas cadambine influences GPCR, PPARG, and EGFR signaling nodes. Lipophilic terpenoids or sterols may aid membrane partitioning, whereas saponins can enhance permeability [41,42].

Translational hurdles and strategies

Cadambine's principal translational barrier is CNS delivery. Its high TPSA and low lipophilicity restrict passive diffusion across the BBB, and efflux mechanisms such as P-glycoprotein may further reduce brain uptake. Strategies to overcome these limitations include medicinal chemistry optimization through prodrug or scaffold modification, as well as formulation-based approaches such as polymeric or lipid nanocarriers, intranasal administration, or receptor-mediated transport systems [43]. In early pharmacology, localized delivery (e.g., intracerebroventricular or intrathecal) could help decouple pharmacodynamics from exposure constraints. Integrating biochemical validation – stronger GR/SOD responses – with network-level hypotheses exemplifies how bottom-up experimental signals refine top-down computational predictions, expediting the path from phytochemical ensembles to tractable CNS candidates.

CONCLUSION

This study integrates network pharmacology, *in silico* ADMET analysis, and *in vitro* biochemical assays to elucidate the neuroprotective potential of cadambine and its congeners from *N. cadamba*. Network mapping identified mechanistically coherent hubs such as CASP3, EGFR, PPARG, MMP2/9, and ADORA1/ADORA2A. They are implicated in apoptosis, neuroinflammation, and redox regulation, supporting a multitarget mode of action rather than single-site inhibition.

Biochemical validation reinforced these predictions: Extracts produced dose-dependent enhancement of GR and SOD activities, particularly in bark fractions, confirming strengthened antioxidant defenses and reduced oxidative stress. Although AChE data remain to be normalized, preliminary activity trends suggest additional cholinergic modulation, aligning with both disease-modifying and symptomatic mechanisms.

Given cadambine's high polarity and limited predicted BBB permeability, formulation-driven strategies such as nanocarriers or intranasal delivery will be critical to achieve effective CNS exposure. Overall, cadambine-family alkaloids emerge as network-acting phytochemicals capable of restoring multiple dysregulated pathways in AD. This integrated computational-experimental framework provides a rational basis for further optimization, mechanistic validation, and translational advancement of *N. cadamba*-derived leads for neurodegenerative therapeutics.

ACKNOWLEDGMENTS

The authors thank the School of Pharmaceutical Sciences, Vels Institute of Science, Technology and Advanced Studies (VISTAS), Chennai, for providing laboratory facilities and technical support.

AUTHORS' CONTRIBUTIONS (CREDIT STATEMENT)

Kavitha M: Conceptualization, Methodology, Investigation, Data Curation, Formal Analysis, Visualization, Writing – Original Draft Preparation. Ronald Darwin C: Supervision, Validation, Resources, Writing – Review and Editing, Project Administration, Correspondence. All authors have read and approved the final version of the manuscript and agree to be accountable for all aspects of the work.

CONFLICT OF INTEREST

The authors declare no competing interests.

FUNDING

This research did not receive any specific grant from funding agencies in the public, commercial, or not-for-profit sectors.

DATA AVAILABILITY

All datasets and computational scripts will be made available upon request.

ETHICAL APPROVAL

The *in vitro* experiments were conducted following institutional biosafety and ethical standards of VISTAS, Chennai.

REFERENCES

1. World Health Organization. Dementia. World Health Organization. Available from: https://www.who.int/news-room/fact-sheets/detail/dementia [Last accessed on 2025 Oct 29].
2. Querfurth HW, LaFerla FM. Alzheimer's disease. N Engl J Med. 2010 Jan 28;362(4):329-44. doi: 10.1056/nejmra0909142, PMID 20107219
3. Hopkins AL. Network pharmacology: The next paradigm in drug discovery. Nat Chem Biol. 2008 Nov;4(11):682-90. doi: 10.1038/nchembio.118, PMID 18936753
4. Sindhu TJ, James JP, Fathima CZ, Vasudevan R, Alegaon SG. Focused insights into Alzheimer's treatment strategies: Pharmacophore modelling, DFT studies, MD simulations and SH-SY5Y neuroprotection of Naringin. Int J Appl Pharm. 2025;17(6):485-98.
5. Pandey A, Negi PS. Traditional uses, phytochemistry and pharmacological properties of *Neolamarckia cadamba*: A review. J Ethnopharmacol. 2016 Apr;181:118-35. doi: 10.1016/j.jep.2016.01.036, PMID 26821190
6. George J, Dhavan P, Jadhav B, Meshram G, Patil V. FT-IR coupled secondary metabolites profiling and biological activities of *Neolamarckia cadamba* leaves. Nat Resour Hum Health. 2022 Oct 30;3(1):94-100. doi: 10.53365/nrfhh/148092
7. Dubey A, Nayak S, Goupale DC. *Anthocephalus cadamba*: A review. Pharmacogn J. 2011 Jan;2(18):71-6. doi: 10.1016/S0975-3575(11)80029-5.
8. Pardridge WM. The blood-brain barrier: Bottleneck in brain drug development. Neurorx. 2005 Jan;2(1):3-14. doi: 10.1602/neurorx.2.1.3, PMID 15717053
9. Li S, Zhang B. Traditional Chinese medicine network pharmacology: Theory, methodology and application. Chin J Nat Med. 2013 Mar;11(2):110-20. doi: 10.1016/S1875-5364(13)60037-0, PMID 23787177
10. Ellman GL, Courtney KD, Andres V Jr., Feather-stone RM. A new and rapid colorimetric determination of acetylcholinesterase activity. Biochem Pharmacol. 1961 Jul;7(2):88-95. doi: 10.1016/0006-2952(61)90145-9, PMID 13726518
11. Dringen R. Metabolism and functions of glutathione in brain. Prog Neurobiol. 2000 Dec;62(6):649-71. doi: 10.1016/S0301-0082(99)00060-X
12. McCord JM, Fridovich I. Superoxide dismutase: The first twenty years (1968-1988). Free Radic Biol Med. 1988;5(5-6):363-9. doi: 10.1016/0891-5849(88)90109-8, PMID 2855736
13. Stelzer G, Rosen N, Plaschkes I, Zimmerman S, Twik M, Fishilevich S. The GeneCards suite: From gene data mining to disease genome sequence analyses. Curr Protoc Bioinformatics. 2016 Jun;54(1):1.30.1-33. doi: 10.1002/cpbi.5, PMID 27322403
14. Daina A, Michielin O, Zoete V. SwissTargetPrediction: Updated data and new features for efficient prediction of protein targets of small molecules. Nucleic Acids Res. 2019 Jul 2;47(W1):W357-64. doi: 10.1093/nar/gkz382, PMID 31106366
15. Venny 2.1.0. Available from: https://bioinfogp.cnb.csic.es/tools/venny [Last accessed on 2025 Oct 29].
16. Szklarczyk D, Gable AL, Lyon D, Junge A, Wyder S, Huerta-

Cepas J. STRING v11: Protein-protein association networks with increased coverage, supporting functional discovery in genome-wide experimental datasets. Nucleic Acids Res. 2019 Jan 8;47(D1):D607-13. doi: 10.1093/nar/gky1131, PMID 30476243
17. Shannon P, Markiel A, Ozier O, Baliga NS, Wang JT, Ramage D. Cytoscape: A software environment for integrated models of biomolecular interaction networks. Genome Res. 2003 Nov;13(11):2498-504. doi: 10.1101/gr.1239303, PMID 14597658
18. Ashburner M, Ball CA, Blake JA, Botstein D, Butler H, Cherry JM. Gene Ontology: Tool for the unification of biology. The gene ontology consortium. Nat Genet. 2000 May;25(1):25-9. doi: 10.1038/75556, PMID 10802651
19. Kanehisa M, Goto S. KEGG: Kyoto encyclopedia of genes and genomes. Nucleic Acids Res. 2000 Jan 1;28(1):27-30. doi: 10.1093/nar/28.1.27, PMID 10592173
20. Benjamini Y, Hochberg Y. Controlling the false discovery rate: A practical and powerful approach to multiple testing. J R Stat Soc Ser B. 1995;57(1):289-300. doi: 10.1111/j.2517-6161.1995.tb02031.x
21. Daina A, Michielin O, Zoete V. SwissADME: A free web tool to evaluate pharmacokinetics, drug-likeness and medicinal chemistry friendliness of small molecules. Sci Rep. 2017 Mar 3;7(1):42717. doi: 10.1038/srep42717, PMID 28256516
22. Daina A, Zoete V. A BOILED-egg to predict gastrointestinal absorption and brain penetration of small molecules. ChemMedChem. 2016 Jun 6;11(11):1117-21. doi: 10.1002/cmdc.201600182, PMID 27218427
23. Banerjee P, Eckert AO, Schrey AK, Preissner R. ProTox-II: A webserver for the prediction of toxicity of chemicals. Nucleic Acids Res. 2018 Jul 2;46(W1):W257-63. doi: 10.1093/nar/gky318, PMID 29718510
24. Marklund S, Marklund G. Involvement of the superoxide anion radical in the autoxidation of pyrogallol and a convenient assay for superoxide dismutase. Eur J Biochem. 1974 Sep;47(3):469-74. doi: 10.1111/j.1432-1033.1974.tb03714.x, PMID 4215654
25. Carlberg I, Mannervik B. Glutathione reductase. Methods Enzymol. 1985;113:484-90. doi: 10.1016/s0076-6879(85)13062-4, PMID 3003504
26. Zhang R, Zhu X, Bai H, Ning K. Network pharmacology databases for traditional Chinese medicine: Review and assessment. Front Pharmacol. 2019 Feb 21;10:123. doi: 10.3389/fphar.2019.00123, PMID 30846939
27. Aoyama K, Nakaki T. Glutathione in cellular redox homeostasis: Association with the excitatory amino acid Carrier 1 (EAAC1). Molecules. 2015 May 14;20(5):8742-58. doi: 10.3390/molecules20058742, PMID 26007177
28. Perry JJ, Shin DS, Getzoff ED, Tainer JA. The structural biochemistry of the superoxide dismutases. Biochim Biophys Acta. 2010 Feb;1804(2):245-62. doi: 10.1016/j.bbapap.2009.11.004, PMID 19914407
29. Hengartner MO. The biochemistry of apoptosis. Nature. 2000 Oct;407(6805):770-6. doi: 10.1038/35037710, PMID 11048727
30. Dwevedi A, Sharma K, Sharma YK. Cadamba: A miraculous tree having enormous pharmacological implications. Pharmacogn Rev. 2015;9(18):107-13. doi: 10.4103/0973-7847.162110, PMID 26392707
31. Misrani A, Tabassum S, Yang L. Mitochondrial dysfunction and oxidative stress in Alzheimer's disease. Front Aging Neurosci. 2021 Feb 18;13:617588. doi: 10.3389/fnagi.2021.617588, PMID 33679375
32. Jurcău MC, Andronie-Cioara FL, Jurcău A, Marcu F, Ţiţ DM, Paşcalău N. The link between oxidative stress, mitochondrial dysfunction and neuroinflammation in the pathophysiology of Alzheimer's disease: Therapeutic implications and future perspectives. Antioxidants (Basel). 2022 Oct 31;11(11):2167. doi: 10.3390/antiox11112167, PMID 36358538
33. Song D, Hao J, Fan D. Biological properties and clinical applications of berberine. Front Med. 2020 Oct;14(5):564-82. doi: 10.1007/s11684-019-0724-6, PMID 32335802
34. Stone TW, Ceruti S, Abbracchio MP. Adenosine receptors and neurological disease: Neuroprotection and neurodegeneration. Handb Exp Pharmacol 2009;193:535-87. doi: 10.1007/978-3-540-89615-9_17
35. Birks JS, Harvey RJ. Donepezil for dementia due to Alzheimer's disease. Cochrane Database Syst Rev. 2018 Jun 18;6(6):CD001190. doi: 10.1002/14651858.CD001190.pub3, PMID 29923184
36. Pohanka M. Cholinesterases, a target of pharmacology and toxicology. Biomed Pap Med Fac Univ Palacky Olomouc Czech Repub. 2011 Sep 1;155(3):219-29. doi: 10.5507/bp.2011.036, PMID 22286807
37. Butterfield DA, Swomley AM, Sultana R. Amyloid β- peptide (1-42)-induced oxidative stress in Alzheimer disease: Importance in disease pathogenesis and progression. Antioxid Redox Signal. 2013 Sep 10;19(8):823-35.
38. Heneka MT, Fink A, Doblhammer G. Effect of pioglitazone medication on the incidence of dementia. Ann Neurol. 2015 Aug;78(2):284-94. doi: 10.1002/ana.24439, PMID 25974006
39. Spagnuolo C, Napolitano M, Tedesco I, Moccia S, Milito A, Russo GL. Neuroprotective role of natural polyphenols. Curr Top Med Chem. 2016 Apr 29;16(17):1943-50. doi: 10.2174/1568026616666160204122449, PMID 26845551
40. Winiarska-Mieczan A, Kwiecień M, Jachimowicz-Rogowska K, Donaldson J, Tomaszewska E, Baranowska-Wójcik E. Anti-inflammatory, antioxidant, and neuroprotective effects of polyphenols-polyphenols as an element of diet therapy in depressive disorders. Int J Mol Sci. 2023 Jan 23;24(3):2258.
41. Chen J, Jiang QD, Chai YP, Zhang H, Peng P, Yang XX. Natural terpenes as penetration enhancers for transdermal drug delivery. Molecules. 2016 Dec 11;21(12):1709. doi: 10.3390/molecules21121709, PMID 27973428
42. Podolak I, Galanty A, Sobolewska D. Saponins as cytotoxic agents: A review. Phytochem Rev. 2010 Sep;9(3):425-74. doi: 10.1007/s11101-010-9183-z, PMID 20835386
43. Martin YC. A bioavailability score. J Med Chem. 2005 May 1;48(9):3164-70. doi: 10.1021/jm0492002, PMID 15857122